Table 1. *Ranges in s corresponding to the number of major oscillations*

s	Number of pronounced oscillations
0–5	1
5–9	2
9–13	3
⋮	⋮
4n−3–4n+1	n

After some simplifications, one obtains the following two solutions

$$\tan(\pi/s)[s^2/4+(h_3^0)^2] = \frac{S[(2/s)^{1/2}(s/2+h_3^0)]+S[(2/s)^{1/2}(s/2-h_3^0)]}{C[(2/s)^{1/2}(s/2+h_3^0)]+C[(2/s)^{1/2}(s/2-h_3^0)]}, \quad (13)$$

$$h_3^0 = \pm\text{integer}.$$

Figs. 3 and 4 give the profile shape *versus* h_3 for s values of 0·10, 14·9, 30·9 and 46·9 (all locate minimum positions in Fig. 1). In Fig. 3, s was increased by fixing N_3 at 1000 and increasing $\Delta d/\langle d\rangle$. The number of oscillations is seen to increase from 0 to 6, in steps of 2. Note that the width of the peak increases with increasing $\Delta d/\langle d\rangle$. As expected, the number of oscillations in the half space with $s \geq 14{\cdot}9$ is equal to the number of pairs of minima (sine, cosine) in the Fresnel functions between $x=0$ and $x=(s/2)^{1/2}$. In Fig. 4, s was increased by fixing $\Delta d/\langle d\rangle$ at 0·01 and increasing N_3. In this case, the width of the peak is a constant, whereas the number of oscillations increases.

It becomes evident from these results that approximate values of $\Delta d/\langle d\rangle$ and N_3 can be determined very simply. If $s>4$, then the ratio of the intensities at $h_3^0=\pm(s/2)[h_3=\pm\frac{1}{2}(\Delta d/\langle d\rangle)l]$ to that at $h_3^0=0(h_3=l)$ is approximately equal to one-fourth. Consequently, the width at one-fourth the intensity of the peak center can be used to estimate $\Delta d/\langle d\rangle$. Similarly, the number of pronounced oscillations in the full X-ray profile is given by int$[(s+3)/4]$ where int denotes 'integer part of'. From the preceding discussion, we have found that the peak width and the number of major oscillations can be used to estimate $\Delta d/\langle d\rangle$ and s. The latter being known N_3 can be calculated. Table 1 gives various ranges in s corresponding to the number of major oscillations. This procedure is only semi-quantitative and is suggested only for a quick interpretation of the intensity data. The most accurate determination of the parameters is obtained by least-squares fitting the experimental profile to (12). This may be carried out by beginning with estimates of $\Delta d/\langle d\rangle$ and N_3.

The authors are grateful to the National Science Foundation (Grant No. DMR-8000933) for funding this research.

References

ABRAMOWITZ, M. & STEGUN, I. (1964). *Handbook of Mathematical Functions.* Washington, DC: US Government Printing Office.
HALL, M. M., VEERARAGHAVEN, V. G., RUBEN, H. & WINCHELL, P. G. (1977). *J. Appl. Cryst.* **10**, 66–68.
HOUSKA, C. R. (1970). *J. Appl. Phys.* **41**, 69–75.
HOUSKA, C. R. (1978). *J. Appl. Phys.* **49**, 2991–2993.
HOUSKA, C. R. & SMITH, T. M. (1981). *J. Appl. Phys.* **52**, 748–754.
NAIDU, W. V. N. & HOUSKA, C. R. (1982). *J. Appl. Cryst.* **15**, 190–198.
WHITE, J. E. (1950). *J. Appl. Phys.* **21**, 855–859.
WILSON, A. J. C. (1949). *Acta Cryst.* **2**, 220–222.

Acta Cryst. (1985). A**41**, 517–528

The Calculation and Interpretation of Multiphonon X-ray Scattering – Example of Cubic Zincblende Structure Compounds

BY JOHN S. REID

Department of Natural Philosophy, The University, Aberdeen AB9 2UE, Scotland

(*Received* 18 *December* 1984; *accepted* 22 *March* 1985)

Abstract

The problems of making calculations using the total phonon scattering cross section in the harmonic approximation are examined and it is found that the method of Reid & Smith [*J. Phys. C* (1970), **3** 1513–1526] can be extended to cope with any material with a modest number of atoms per unit cell. Complex eigenvectors and complex scattering factors may be handled without approximations. The method is used to evaluate the multiphonon scattering (and one-phonon scattering) for a number of cubic zincblende structure compounds including GaAs, CdTe, CuI and SiC, taking eigendata from good lattice dynamical models. The results illustrate a discussion of the typical behaviour of multiphonon scattering as a

0108-7673/85/060517-12$01.50

function of scattering vector and temperature. The effect of anomalous dispersion on the total phonon scattering cross section is also shown and a discussion given of the origin of multiphonon processes, with particular reference to the contribution of these processes to the diffuse scattering observed near Bragg reflections. It is also concluded that dynamic deformation will not significantly affect multiphonon intensities.

Introduction

The normal approach to phonon scattering of X-rays in the harmonic approximation is to express the total cross section as a series of terms, the terms representing one-phonon scattering, two-phonon scattering, three-phonon scattering and so on. These terms are increasingly tedious to calculate, so much so that an exact calculation of the three-phonon terms is seldom attempted and resort is made to drastic approximations for higher-order terms. The difficulties of evaluating these sums for a zincblende structure material are well illustrated for InAs by Orlova (1979*a*, *b*, 1981).

So widespread is the phonon expansion and its subsequent limit to one or two terms that it is generally taken for granted (for any material) that (*a*) three-phonon and higher-order terms are negligible and (*b*) if one is sufficiently concerned to bother about multiphonon scattering it is so structureless in reciprocal space that it can be represented by the incoherent approximation. Regrettably both these working rules are generally false. The phonon expansion is satisfactory only in the regime where the series converges very rapidly, quite seriously limiting the range of scattering vectors and temperatures where it can be reasonably applied.

The analytic expression for the total phonon scattering, including all multiphonon processes in the harmonic approximation, has been known since the work of Waller (1928), and more widely since the article by Born (1942) and the textbook by Maradudin, Montroll & Weiss (1963). Reid & Smith (1970) demonstrated that it was feasible in the case of an alkali halide to calculate precisely the total cross section from a good lattice dynamical model. Since that time little progress has been made in extending their technique to more complex materials. Robertson & Reid (1978) presented the results of a corresponding calculation using a shell model for silicon but gave no details of their treatment. It is worth returning again to the work of Reid & Smith (1970), for several reasons:

(*a*) to refine the method and extend it to more complex materials;

(*b*) to point out the possibilities and limitations of their approach;

(*c*) to explore more fully the features of the *total phonon scattering* that are representative of materials in general, particularly with regard to variation of scattering vector and temperature;

(*d*) to calculate results for the important class of materials represented by the cubic zincblende structure materials [for example to help interpret the experimental work of Ghezzi & Bocchi (1982)];

(*e*) to use it to investigate the sort of differences in the scattering that can be given by different 'good' lattice dynamical models for the same material.

These aspects will be dealt with here, along with some account of the relevance of multiphonon processes in the integrated diffuse scattering intensity measured around Bragg peaks.

The total scattering cross section

The kinematic harmonic X-ray scattering cross section for scattering vector **K** is given in electron units per cell (following Maradudin *et al.*, 1963 and others) as

$$I/N\sigma_0 I_0 = \sum_{lkk'} f_k \exp(-W_k) f_{k'}^* \exp(-W_{k'}) \times \exp\{i\mathbf{K}.[\mathbf{r}(lk)-\mathbf{r}(0k')]\} \exp(W_{kk'}) \quad (1a)$$

where

$$W_{kk'} = (1/2N) \sum_{\lambda} (E/\omega^2)_\lambda \times \{[\mathbf{K}.\mathscr{E}(k/\lambda) m_k^{-1/2}][\mathbf{K}.\mathscr{E}^*(k'/\lambda) m_{k'}^{-1/2}] + [\mathbf{K}.\mathscr{E}^*(k/\lambda) m_k^{-1/2}][\mathbf{K}.\mathscr{E}(k'/\lambda) m_{k'}^{-1/2}]\} \times \exp\{i\mathbf{q}.[\mathbf{r}(lk)-\mathbf{r}(0k')]\}. \quad (1b)$$

The notation is one variant of common practice and is given for reference in the Appendix.

Expression (1) is the basis for the calculations reported here. The Debye–Waller factors appear explicitly and have often been considered as parameters that can be determined from Bragg scattering intensities. Expression (1) is also the basis for the traditional phonon expansion, achieved by representing $\exp(W_{kk'})$ as a power series of phonon sums. In this paper the term 'multiphonon' refers to the sum of all phonon processes except the one-phonon.

It is worth noting that the total phonon scattering may be written in a slightly different form, which will be more helpful for interpreting some aspects of the origin and behaviour of multiphonon scattering. The separation of the Debye–Waller terms W_k from the exponent $W_{kk'}$ is a separation of habit and some convenience, rather than a necessity. Both are controlled by the same lattice dynamical properties. They may be combined succinctly to give the total

scattering as

$$I/N\sigma_0 I_0 = \sum_{lkk'} f_k f_{k'}^* \exp\{i\mathbf{K}.[\mathbf{r}(lk)-\mathbf{r}(0k')]\} \times \exp\{-(1/2N)\sum_{\lambda}(E/\omega^2)_\lambda \times |\mathbf{K}.\mathscr{E}(k/\lambda)m_k^{-1/2}\exp[i\mathbf{q}.\mathbf{r}(lk)] - \mathbf{K}.\mathscr{E}(k'/\lambda)m_{k'}^{-1/2}\exp[i\mathbf{q}.\mathbf{r}(0k')]|^2\}. \quad (2)$$

Expressions (1) and (2) are identical if the Debye-Waller factors are calculated from the same eigendata as those used to evaluate $W_{kk'}$ but otherwise they are not, with implications that will be discussed later. Expression (2) also shows that the Debye-Waller factor represents a reduction in scattering caused by a particular set of multiphonon processes that involve no net change in the scattering vector. Viewed in this light, these are the multiphonon effects with which crystallographers are most familiar. It is natural from this viewpoint to ask what scattering effects are produced by all other multiphonon processes. Those who are not interested in the calculations themselves should move to the section on *The structure of the total phonon scattering in reciprocal space.*

Role of the microcrystal

The intensity given by (1) is the scattering given by the entire crystal, the summations being over each atom in the structure and each normal mode. The usual lattice dynamical periodic boundary conditions are implied to remove difficulty with surface atoms. To calculate the scattering, a microcrystal must be chosen. For a given choice of microcrystal its set of phonon wavevectors will constitute a sample of the wavevectors of a macroscopic crystal, uniformly covering the Brillouin zone. Every phonon process represented in the calculation will involve only these wavevectors. This applies to the one-phonon process as well, and hence only a discrete set of scattering vectors **K** can be used in the calculation, namely those that satisfy

$$\mathbf{K}+\mathbf{q}=\mathbf{G}, \quad (3)$$

where **G** is a reciprocal-lattice vector and **q** a wavevector of the microcrystal. The main limiting effect of the microcrystal is this restriction on the allowed scattering vectors for which cross sections can be calculated directly. Scattering cross sections for other **K** values must be obtained by interpolation.

It is a relatively minor effect that in the almost continuous range of wavevectors of a macroscopic crystal there are many between those of the sampled set that are not included in the sum. So long as the sample density is reasonable [in terms of the curvature in reciprocal space of the terms that contribute to the sum $W_{kk'}$ of (1*b*)], the averaging by the sample will adequately represent multiphonon processes. 'Reasonable' appears in practice as 500 wavevectors distributed through the Brillouin zone (see later).

Reid & Smith chose a microcrystal consisting of n by n by n face-centred-cubic unit cells. This has $4n^3$ wavevectors and is a satisfactory choice for values of $n=5$ and above. As an alternative to this 'cubic' choice, a 'primitive' microcrystal consisting of $2n$ by $2n$ by $2n$ primitive unit cells is also used in the calculations here (Fig. 1). This has $8n^3$ wavevectors and gives a better coverage of scattering vectors in some directions. For example in the [111] direction, scattering vectors in increments of $(0{\cdot}2, 0{\cdot}2, 0{\cdot}2)2\pi/d$ are given by a cubic microcrystal with $n=5$ but increments of $(0{\cdot}1, 0{\cdot}1, 0{\cdot}1)2\pi/d$ are obtained from the primitive microcrystal with $n=5$. Since the primitive microcrystal has twice the number of wavevectors and twice the number of atoms, the calculation takes four times as long. To obtain the same finer spacing with a cubic microcrystal requires $n=10$ and hence a calculation taking 64 times as long.

Role of symmetry

The cubic symmetry of the zincblende structure materials provides no major simplification of the summation, because symmetry-related wavevectors do not produce symmetry-related contributions to $W_{kk'}$ owing to the presence of the real lattice coordinate $\mathbf{r}(lk)$. Although hindering the calculations in this case, the implication is that materials of much lower symmetry can be likewise treated. The inversion symmetry of every Bravais lattice (and reciprocal lattice) allows the $\mathbf{r}(lk)$ and **q** sums to be taken over half the number of points. The contribution of pairs of terms

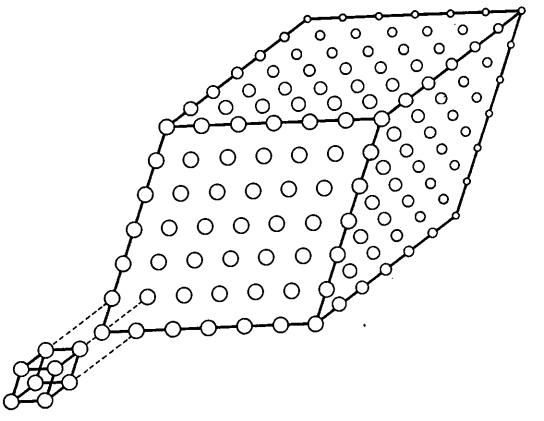

Fig. 1. The primitive microcrystal with $n=3$, which contains $(2n)$ primitive f.c.c. unit cells. The bottom left atom is taken as at coordinate $(-n, -n, -n)d$ and the top right as at $(n, n, n)d$, where d is the cubic cell side.

to $W_{kk'}$ becomes

$$[2/N(m_k m_{k'})^{1/2}]\sum_j (E/\omega^2)_\lambda \{[\mathbf{K}.\mathscr{E}^r(k/\lambda)\mathbf{K}.\mathscr{E}^r(k'/\lambda) + \mathbf{K}.\mathscr{E}^i(k/\lambda)\mathbf{K}.\mathscr{E}^i(k'/\lambda)]\cos\mathbf{q}.[\mathbf{r}(lk)-\mathbf{r}(0k')] + [\mathbf{K}.\mathscr{E}^i(k/\lambda)\mathbf{K}.\mathscr{E}^r(k'/\lambda) - \mathbf{K}.\mathscr{E}^r(k/\lambda)\mathbf{K}.\mathscr{E}^i(k'/\lambda)]\sin\mathbf{q}.[\mathbf{r}(lk)-\mathbf{r}(0k')], \quad (4)$$

where the superscripts r and i refer to the real and imaginary parts of the eigenvectors.

Anomalous dispersion

Anomalous dispersion modifies the scattering factors f_k to complex

$$f_k = f_k^0 + f_k' + if_k'', \quad (5)$$

where f_k^0 is the uncorrected scattering factor, f_k' and f_k'' the anomalous corrections. Values for f_k' and f_k'' listed in *International Tables for X-ray Crystallography* (1974) were used in the results presented later, but it is straightforward to use experimental values. They are accurately incorporated by writing the *total* scattering factor in the complex notation

$$f_k = |f_k| \exp(i\varphi_k). \quad (6)$$

The scattering-factor phase difference is added into the real-space cosine terms (arising from the Bravais-lattice inversion symmetry), giving them as

$$2\cos\{\mathbf{K}.[\mathbf{r}(lk)-\mathbf{r}(0k')]+\varphi_k-\varphi_{k'}\} \quad (7)$$

and $|f_k|$ used in (1) to multiply the Debye–Waller term. The accuracy of the anomalous dispersion coefficients may fall short of that of the scattering factors but their inclusion does show (for the first time?) the effect of anomalous dispersion on multiphonon scattering.

There is nothing special about the complexity introduced by anomalous scattering. The same approach may be used to incorporate complexity of the scattering factors from any other cause (such as a non-spherical electron distribution) without any increase in computing time.

Zerophonon term

The occurrence of the term $\mathbf{q}=0$ in the total phonon scattering equation (1) cannot be taken at face value, nor be omitted on the grounds that the real sample is held stationary in the laboratory. It must be argued that the microcrystal successfully represents the scattering from a real crystal because contributions from each wavevector of the microcrystal accurately represent the average contribution from a surrounding volume of wavevectors that are present in the scattering sums for a much larger crystal. Hence the single contribution from $\mathbf{q}=0$ in the microcrystal should represent the average contribution from a surrounding volume (of very small wavevectors). Reid & Smith evaluated this 'zerophonon' term from the macroscopic data of elastic constants and optical frequencies (at zero wavevector). It is more consistent to evaluate the zerophonon term from the lattice dynamical model used for the rest of the phonon data. This will be done here. It is also important to give it thorough attention because this one term provides a disproportionate contribution to the scattering. In fact as the Bragg peak is approached it provides a greater and greater fraction of the total scattering, typically reaching in excess of 20% at the closest point to the Bragg peak for the microcrystals considered here.

Let the zerophonon contribution to $W_{kk'}$ of (1*b*) be $Z_{kk'}$, then

$$Z_{kk'} = [1/N(m_k m_{k'})^{1/2}]\sum_j (1/V_Z) \times \int_{V_Z} \mathrm{d}\mathbf{q}\,(E/\omega^2)_\lambda \mathbf{K}.\mathscr{E}(k/\lambda)\mathbf{K}.\mathscr{E}^*(k'/\lambda), \quad (8)$$

where V_Z is the 'zerophonon volume' of $1/N$th the Brillouin zone volume. Since the phase term in $W_{kk'}$ does not differ much from unity over the microcrystal zerophonon volume, the factor $\exp(Z_{kk'})$ multiplies the entire scattering sum calculated over the remainder of the Brillouin zone, giving the zerophonon contribution to the scattering as

$$\sum_{kk'}[\exp(Z_{kk'})-1] \times (\text{scattering due to rest of phonons}). \quad (9)$$

In distinction to the general term contributing to $W_{kk'}$, cubic symmetry of the zincblende structure materials does simplify the zerophonon term. Equation (8) becomes

$$Z_{kk'} = [1/N(m_k m_{k'})^{1/2}](|K|^2/3)\sum_j (1/V_Z) \times \int_{V_Z} \mathrm{d}\mathbf{q}(E/\omega^2)_\lambda \mathscr{E}(k/\lambda).\mathscr{E}^*(k'/\lambda). \quad (10)$$

From this expression the zerophonon term is evaluated under the following assumptions:

(*a*) The zerophonon volume is a sphere of radius r_z (equal to $1/N$th the Brillouin zone volume);

(*b*) within the zerophonon volume the optic branches are constant, the acoustic branches dispersionless, and the eigenvectors constant in any direction;

(*c*) the variation of slope in the acoustic branches with direction of wavevector may be represented by a sample of a star of the smallest wavevectors.

Following (*c*) the zerophonon volume is divided into $\mathcal{N}_s$ cones, each cone centred on a wavevector $\mathbf{q}_s$ chosen to represent part of the dispersionless limit. The optic mode contribution is therefore

$$ZO_{kk'} = [K^2/3N(m_k m_{k'})^{1/2}] \times \sum_{j_{\text{optic}}} (1/\mathcal{N}_s) \sum_{\mathbf{q}_s} (E/\omega^2)_{\mathbf{q}_s j_{\text{optic}}} \times \mathscr{E}(k/\mathbf{q}_s j_{\text{optic}}) \cdot \mathscr{E}^*(k'/\mathbf{q}_s j_{\text{optic}}) \quad (11)$$

and since all symmetry-related $\mathbf{q}_s$ contribute identically it is only necessary to sum over symmetry-unrelated $\mathbf{q}_s$, provided their multiplicity is accounted for. For the acoustic term, the energy integral must be integrated along $\mathbf{q}_s$ to the edge of the zerophonon volume, which introduces the Debye integral $D(\mathbf{q}_s j_{\text{acoustic}})$ given by

$$D(\mathbf{q}_s j_{\text{acoustic}}) = (1/x_{\max}) \int_0^{x_{\max}} [x/(e^x - 1)]\, dx \quad (12)$$

where

$$x_{\max} = \hbar\omega_{\max}/kT$$

and $\omega_{\max}$ is the angular frequency at the edge of the zerophonon sphere in direction $\mathbf{q}_s$ for the branch j_{acoustic}. The acoustic contribution to the zerophonon volume is now

$$ZA_{kk'} = [K^2/3N(m_k m_{k'})^{1/2}] \times \sum_{j_{\text{acoustic}}} (1/\mathcal{N}_s) \sum_{q_s} [(3kT/\omega^2_{\max}) \times D(\mathbf{q}_s j_{\text{acoustic}}) + 3\hbar/4\omega_{\max}] \times \mathscr{E}(k/\mathbf{q}_s j_{\text{acoustic}}) \cdot \mathscr{E}^*(k'/\mathbf{q}_s j_{\text{acoustic}}). \quad (13)$$

Combination of the constituents (11) and (13) of the zerophonon term gives, simply,

$$Z_{kk'} = ZA_{kk'} + ZO_{kk'} \quad (14)$$

with (9) illustrating how $Z_{kk'}$ appears in the calculation.

The choice of $\mathbf{q}_s$ is a matter of balancing the convenience of a small choice against reasonable accuracy. In the calculations described here, for a microcrystal with $n = 10$ or above the lowest seven symmetry-unrelated wavevectors in the primitive mesh sample were used (giving a star of 122 wavevectors) and below $n = 10$ only the lowest three wavevectors of the primitive mesh (giving a star of 26 wavevectors). Of course eigendata could be specially generated in the zerophonon volume at a much higher density than that given by the mesh being used in the sum, but the procedure outlined above works satisfactorily, as will be seen in the next section.

The same zerophonon technique may be used in Debye–Waller factor calculations.

It is necessary to go through this treatment of the zerophonon term (or an equivalent treatment) if one uses (1) to calculate the scattering. It is not necessary to do so using (2). The zerophonon contribution to the scattering in this formulation is $I(Z)$ given by

$$I(Z)/N\sigma_0 I_0 = \sum_{lkk'} f_k f^*_{k'} \exp\{i\mathbf{K} \cdot [\mathbf{r}(lk) - \mathbf{r}(0k')]\} \times \exp[-(|K|^2/3N) \sum_j (1/V_Z) \times \int_{V_Z} d\mathbf{q}\, (E/\omega^2)_\lambda |\mathscr{E}(k/\lambda)/m_k^{1/2} - \mathscr{E}(k'/\lambda)/m_{k'}^{1/2}|^2]. \quad (15)$$

For all $\mathbf{r}(lk)$, the scattering $I(Z)$ is identically zero for terms with $k' = k$ and small for terms $k' \neq k$. What is happening is that the zerophonon contribution to the scattering [as defined by (9)] is effectively cancelled by the zerophonon contribution to the Debye–Waller factors. Some further implications of this viewpoint will be made later in respect of Bragg reflections.

Results – convergence for increasing microcrystal size

The results presented hereafter have all been calculated with the *cubic* microcrystal choice of $n = 10$ for scattering vectors in the [100] and [110] directions and with the *primitive* microcrystal of $n = 10$ for the [111] direction. In general the Debye–Waller factors appropriate to the model as calculated by Reid (1983*a*) were used but for GaAs at 295 K the best experimental values ($B_{\text{Ga}} = 0{\cdot}686$; $B_{\text{As}} = 0{\cdot}575$; G. Mackintyre, private communication) were chosen for all models to try to improve the accuracy of the intensities at lower wavevectors (see later).

Results calculated for small microcrystals agree with those for larger ones even better than might be anticipated. For example the zone boundary scattering (where the multiphonon contribution is the greatest percentage of the total) is given in GaAs to within a few percent by the extremely small microcrystal of three unit face-centred cubes along each edge. Table 1 shows some convergence figures for different mesh sizes. It also illustrates that within the practical limit of a mesh size of $n = 20$ (dictated by a computing requirement of roughly 10^{10} floating-point operations) convergence can only be checked without interpolation at the relatively small set of **K** values that are commensurate with several meshes.

There are several reasons for this good convergence. The periodic boundary conditions ensure that the bulk phonon frequencies and eigenvectors are always used; at both small and large $\sin\theta/\lambda$ the total phonon scattering is necessarily independent of the mesh, as is discussed in the next section; at intermedi-

Table 1. *The convergence with increasing mesh size of multiphonon scattering intensities (in electron units per cell) for three scattering vectors* **K** *along the* [100] *direction*

The upper figure for each **K** is the multiphonon scattering calculated on the cubic mesh for the given n values; the lower figure, the zerophonon contribution to the above figure. The values marked with * could not be calculated directly but were obtained by four-point interpolation; those marked with † were obtained by three-point interpolation. For $n=5$ the convergence, as a percentage of the multiphonon scattering, is usually better than 1% over the **K** region of interest and as a percentage of the total phonon scattering much better. The figures are for GaAs at 295 K, calculated from the shell model.

K \ n	2	3	4	5	8	10	12	15	16
5·0, 0, 0	17·09	14·58	14·39	14·30	14·27	14·30	14·29	14·29	14·29
	3·72	1·69	1·08	0·80	0·46	0·38	0·31	0·23	0·22
4·5, 0, 0	19·31	17·95†	17·47	17·45*	17·37	17·42	17·41	17·41*	17·41
	6·09	3·36†	1·91	1·47*	0·81	0·67	0·54	0·42*	0·39
4·2, 0, 0				24·53	25·57*	25·83	25·74*	25·93	25·92*
				5·91	3·79*	2·81	2·01*	1·77	1·63*

ate $\sin\theta/\lambda$ values, there is no strong structure over the Brillouin zone in the terms contributing to $W_{kk'}$, and the zerophonon term gives an analytic treatment to long-range correlations in atomic positions that would be most seriously misrepresented by a small microcrystal.

The structure of the total phonon scattering in reciprocal space

Before looking in detail at the numerical results to be presented here, the general structure of the scattering in reciprocal space merits some discussion. Fig. 2, calculated for GaAs at 295 K, shows on a logarithmic scale the broad features to be expected when investigating an appreciable distance along any direction of scattering vector. The one-phonon scattering rises from a non-zero value at small $\sin\theta/\lambda$ showing the expected peaking at Bragg reflections and a decay to ever smaller values at large $\sin\theta/\lambda$ as the Debye–Waller exponent overcomes the K^2 dependence of the one-phonon cross section. The behaviour of the multiphonon scattering is less well known.

Rising from zero at zero $\sin\theta/\lambda$ it too shows appreciable structure as it overtakes the one-phonon

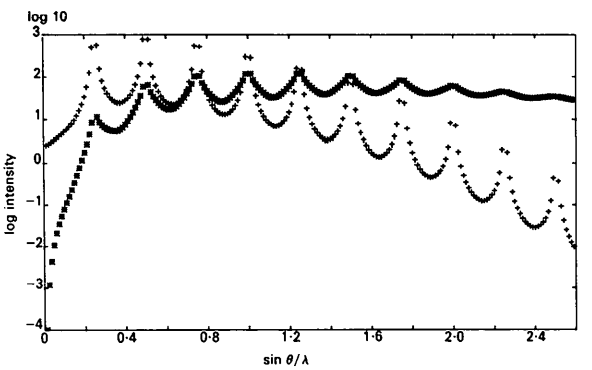

Fig. 2. Variation in one-phonon (+) and multiphonon (*) scattering with $\sin\theta/\lambda$ (Å^{-1}) for scattering vector along [110]. The logarithmic intensities (in electron units per cell) were calculated from the shell model for GaAs at 295 K.

cross section at quite modest $\sin\theta/\lambda$. At $\sin\theta/\lambda$ around 2 Å^{-1}, the structure becomes less pronounced but the multiphonon cross section is *not* eventually reduced by the Debye–Waller factor. In the graph shown it actually flattens off but this is an artifice of the parameterization of the scattering-factor curves in *International Tables for X-ray Crystallography*. This parameterization is only representative for $\sin\theta/\lambda <$ 2 Å^{-1} and contains a constant term, independent of $\sin\theta/\lambda$. It is this constant term that is holding up the large $|\mathbf{K}|$ end of Fig. 3 because in the limit of large $|\mathbf{K}|$

$$I/N\sigma_0 I_0 \rightarrow \sum_k f_k f_k^*, \tag{16}$$

the incoherent approximation.

It is not obvious at first sight how the structure disappears from the multiphonon sum at large $|\mathbf{K}|$ because all terms in the exponent for $W_{kk'}$ appear to be equally affected by an increase in $|\mathbf{K}|$. It is best to look at (2). All terms contributing to the real exponent decrease as $\exp(-\alpha K^2)$, α a constant, except for one. This is the term where $\mathbf{r}(lk)=0$ and $k'=k$. Its exponent is identically 0 for all **K** and hence the scattering at large $|\mathbf{K}|$ is dominated by this one term, which gives just the incoherent sum of (16). 'Multiphonon' is a misnomer for this scattering because no phonons are involved. In this limit, since there is no interference of waves scattered by neighbouring atoms, the mere translational motion of the scattering centres does not influence the cross section. As one comes in from the large $|\mathbf{K}|$ limit (say $\sin\theta/\lambda = 3$ Å^{-1}) scattering from a few other atoms in the crystal begins to influence the intensity. First to come in is the scattering from the neighbouring atom in the unit cell, soon followed by atoms in neighbouring unit cells. Whether these increase or decrease the total cross section depends on the sign of the associated phase terms $\exp\{i\mathbf{K}.[\mathbf{r}(lk)-\mathbf{r}(0k')]\}$. As $|\mathbf{K}|$ reaches modest and small values a great many lk terms are all contributing significantly to the total phonon scattering, which gradually makes a transition from being controlled by one term in real space to being con-

trolled by one term in reciprocal space, the one-phonon scattering.

Two important conclusions can be drawn from this analysis. If Debye-Waller factors are taken from experiment or from some other model (or even from the same model evaluated with a different mesh size) for the calculation, they will not produce the required zero exponent of the term with $\mathbf{r}(lk) = 0$, $k' = k$. The residual exponent will cause the large $|\mathbf{K}|$ scattering to increase or decrease with a spurious exponential factor (depending on whether the Debye-Waller terms are smaller or larger than the model's). The exact value of $|\mathbf{K}|$ at which this spurious term becomes apparent will depend on the mismatch of Debye-Waller values. As an example will show in the next section, this effective alteration of the baseline for multiphonon scattering at larger $|\mathbf{K}|$ can be significant. A second point is that we now have a good justification for seeing that serious errors will not be introduced into the real-space sum by using a small microcrystal to calculate multiphonon scattering in the regime where it is important.

It should be added that all the effects discussed above as depending on $|\mathbf{K}|$ are determined by $\sin\theta/\lambda$ and not by the index of the reflection in units of $2\pi/d$.

Variation of scattering with scattering vector, temperature and material

Looking in some detail along the three principal symmetry directions of GaAs one can see notable variations from the general behaviour. The very weak 200 and 600 reflections show in Fig. 3(*a*) a negligible peaking of the phonon scattering. The same structure factor that is responsible for the weakness of the reflections also reduces the long-wavelength acoustic scattering, which is the dominant phonon scattering process close to Bragg reflections. In general, though, it is not possible to say how much scattering comes from acoustic branches and how much from optic branches. The reason is that for most phonons the distinction between optic and acoustic branches is irrelevant. Indeed the distinction cannot generally be found by examining the frequencies and eigenvectors alone, because branches may cross, but only by connectivity arguments not easy to establish in practice. Of the three main symmetry axes, it is only along the [111] direction that the structure factor can take the full range of values. In Fig. 3(*c*), it can be seen that as 666 is approached the total thermal diffuse scattering actually decreases appreciably. This really will be the structure of the scattering seen by a detector of normal size, even if there is a very narrow one-phonon peak not visible at the resolution of the calculation. Such behaviour is contrary to common assumptions about how the diffuse scattering always varies close to Bragg reflections.

Although rising temperatures rapidly pull intensity out of the larger-index Bragg reflections, owing to the Debye-Waller factor, there is only a modest rise in the thermal scattering at larger $\sin\theta/\lambda$. See Fig. 4. This is because most of the scattering is 'multiphonon scattering' whose baseline of (16) is temperature independent. At low $|\mathbf{K}|$ most of the scattering is one-phonon scattering and this rises directly with temperature once the energy term has reached the high-temperature limit for each contributing phonon state (the Debye-Waller factor being too small to have much effect). More noticeable than differences in general levels is the marked difference in the rela-

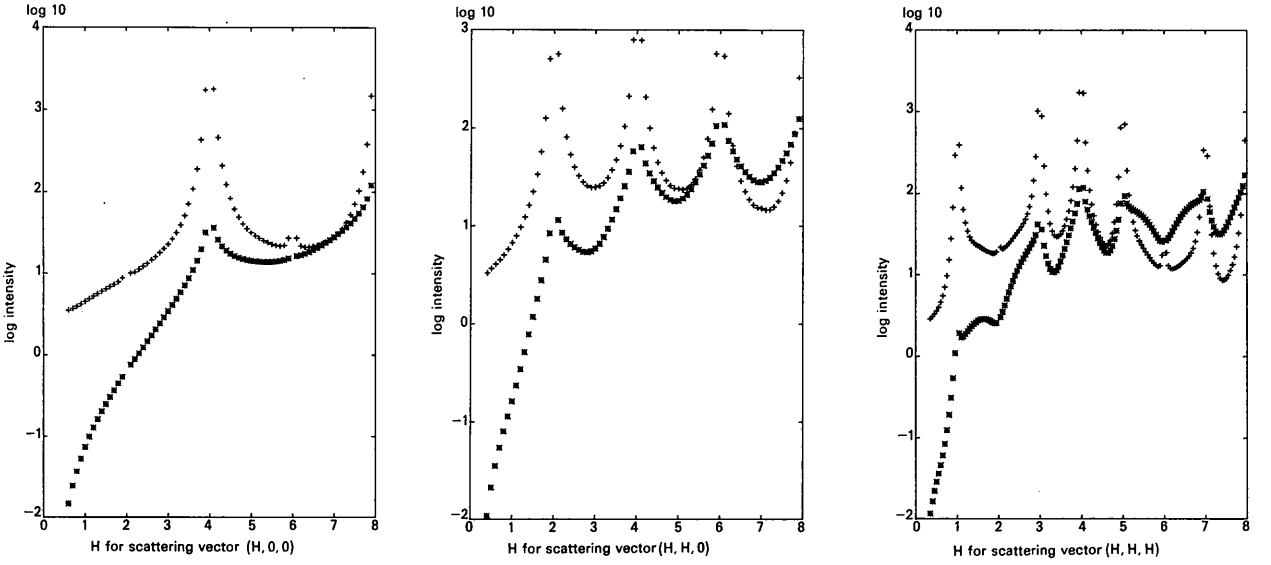

Fig. 3. Variation in one-phonon (+) and multiphonon (*) intensities (in electron units per cell) calculated from the shell model for GaAs at 295 K along (*a*) [100] direction; (*b*) [110] direction; and (*c*) [111] direction.

tive value of multiphonon and one-phonon processes at different temperatures. At low temperatures the multiphonon scattering freezes out rapidly for all but the largest scattering vectors. At high temperatures, multiphonon scattering rises so rapidly with scattering vector that it is generally the dominant process. Fig. 4(*c*) shows, for example, that it equals the one-phonon scattering by 2·5, 2·5, 2·5 at 700 K for GaAs. Notice the very rapid fall off in the one-phonon intensity due to the large Debye–Waller factor at this elevated temperature.

Other materials show similar patterns to GaAs but with variation of fine detail and, in particular, variation of sin θ/λ at which the multiphonon intensity becomes comparable with the one-phonon intensity and at which the one-phonon intensity begins to fall rapidly. Fig. 5 shows as representative of some other sphalerite structure materials the room-temperature scattering given by lattice dynamical models for CdTe, CuI and SiC along the [111] direction. For the sources of all models used in this paper, see Reid (1983*a*).

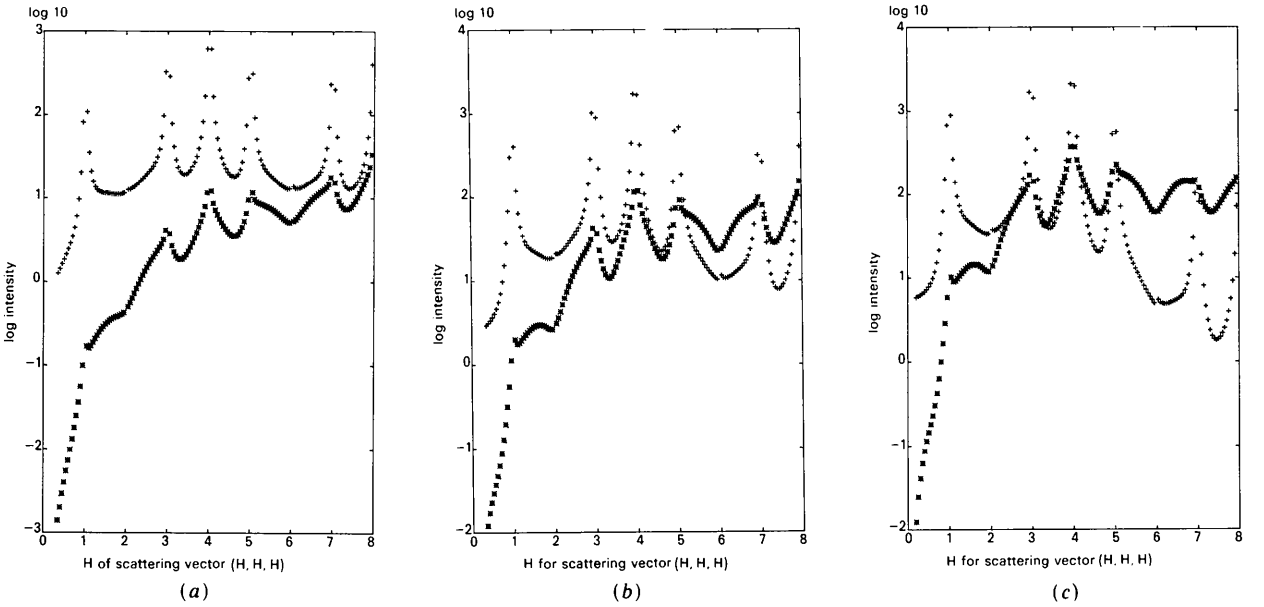

Fig. 4. Variation in one-phonon (+) and multiphonon (*) intensities (in electron units per cell) calculated from the shell model for GaAs with scattering vector along [111] at temperatures of (*a*) 77 K; (*b*) 300 K; and (*c*) 700 K.

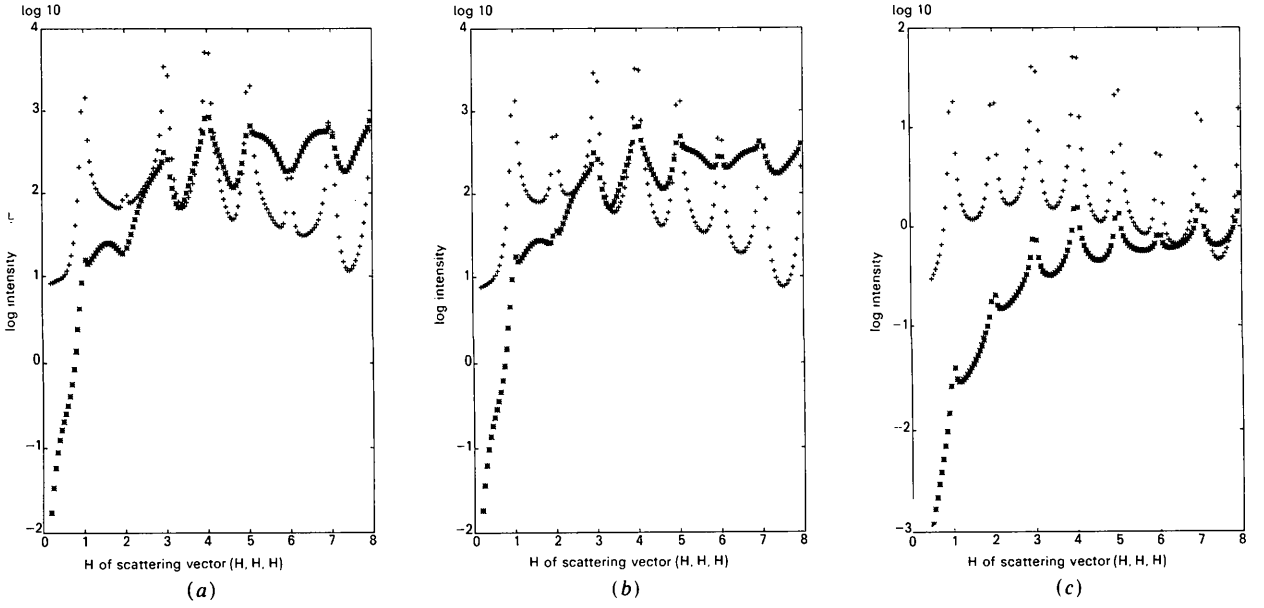

Fig. 5. Variation in one-phonon (+) and multiphonon (*) intensities (in electron units per cell) calculated at 295 K for scattering vector along [111] for (*a*) CdTe from shell model I; (*b*) CuI from the shell model; and (*c*) for SiC from the deformation-dipole model. For references to the models, see Reid (1983*a*).

Anomalous thermal scattering

For the materials considered here, anomalous scattering produces a difference of intensity between Bivjoet pairs only for odd-index Bragg reflections and not for even ones. Along the ⟨100⟩ directions and ⟨110⟩ directions, the diffuse scattering is independent of direction but along ⟨111⟩ and in a general direction intensities are different under the transformation $\mathbf{K} \rightarrow -\mathbf{K}$. Fig. 6 shows the percentage difference in the total diffuse scattering (one-phonon plus multiphonon) between scattering along $[\bar{1}\bar{1}\bar{1}]$ and [111] for GaSb in Cu $K\alpha$ radiation and GaAs in Mo $K\alpha$ radiation. Anomalous scattering factors from *International Tables for X-ray Crystallography* (1974) were used. For GaSb, the large f'' correction at Cu $K\alpha$ for the Sb ion is responsible for the large effects. GaAs at Mo $K\alpha$ is more typical.

Comparison between lattice dynamical models

An earlier study by the author on the Debye–Waller factors predicted by various 'good' lattice dynamical models for the cubic zincblende structure materials concluded that different models gave widely different Debye–Waller factors and that the principal cause appeared to lie with the different eigenvectors predicted by these models (Reid, 1983*a*). It is therefore not particularly surprising to find appreciable differences in the phonon scattering predicted by a variety of models. Taking GaAs as an example, the shell model comes closest to predicting the observed Debye–Waller B_k values but it is not particularly good. Fig. 7 shows the difference between the shell-model diffuse scattering and that for the valence-shell model, the deformation-dipole model and the rigid-ion model along one scattering-vector direction when

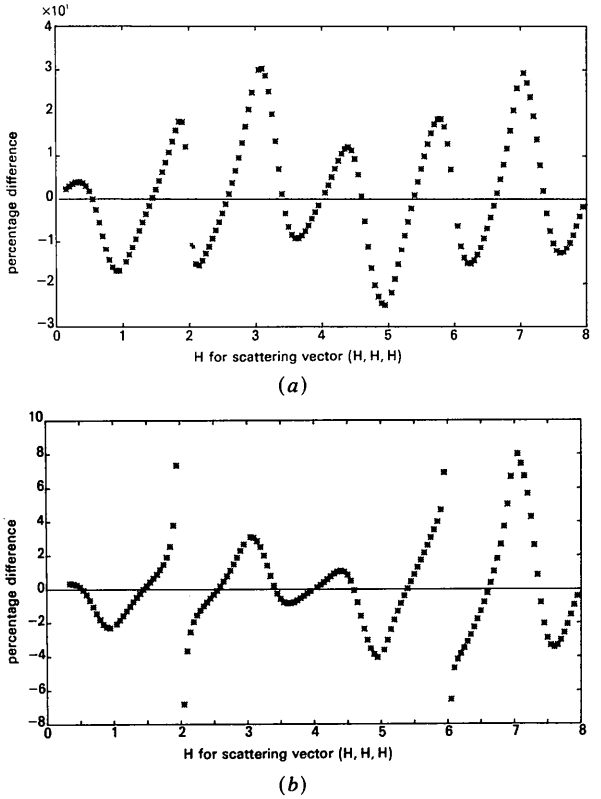

Fig. 6. Percentage difference between total scattering in $[\bar{1}\bar{1}\bar{1}]$ and [111] directions at 295 K for (*a*) GaSb with Cu $K\alpha$ radiation and (*b*) GaAs with Mo $K\alpha$ radiation. The one-phonon and multiphonon scattering individually follow very similar trends.

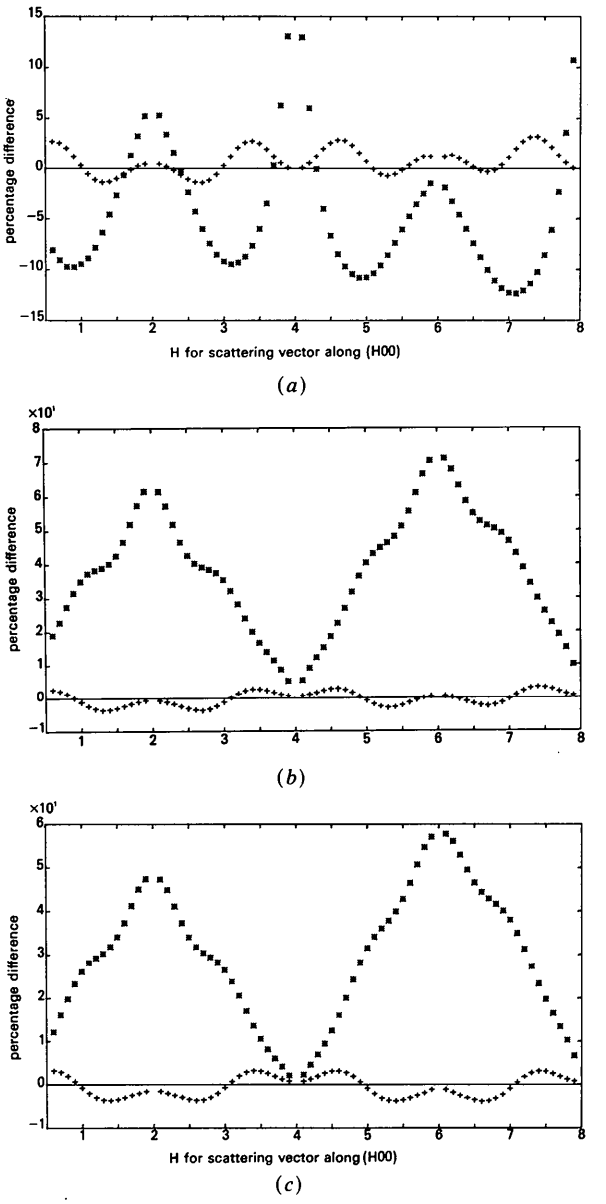

Fig. 7. Percentage difference in one-phonon (+) and multiphonon (*) scattering for GaAs at 295 K along [100] between (*a*) valence-shell model and shell model; (*b*) deformation-dipole model and shell model and (*c*) rigid-ion model and shell model. For all the models the experimental Debye–Waller B values were used (see text).

the experimental Debye–Waller B_k values are used with all models. Sometimes the differences are greatest at Bragg reflections; at other times at zone boundaries. The multiphonon scattering does not follow the same trend as the one-phonon.

In one sense Fig. 7 does not reflect the true difference in scattering predicted by the models because of the use of the experimental Debye–Waller factors. From the earlier discussion it will be seen that it is a matter of some debate as to whether one should treat the Debye–Waller B values as separable parameters in the total phonon scattering. Fig. 8(b) shows the true difference in scattering predicted by the deformation-dipole and shell models when the Debye–Waller terms are treated as part of the model calculation. Comparison should be made with Fig. 8(a), the corresponding difference when the experimental B values are used, to see that the expected improvement in agreement of the multiphonon scattering at large $\sin\theta/\lambda$ does now occur, as the model-independent incoherent limit of (16) is approached. The large difference in one-phonon scattering near 666 reflects a feature of the deformation-dipole model eigenvectors in the [111] direction.

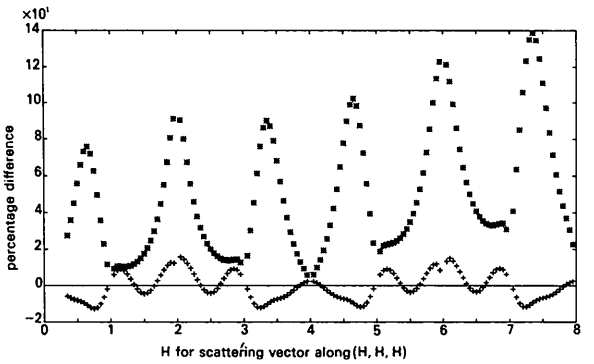

(a)

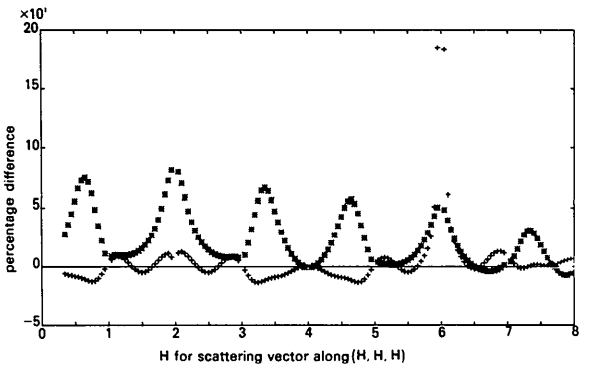

(b)

Fig. 8. Percentage difference in one-phonon (+) and multiphonon (*) scattering for GaAs at 295 K along [111] between deformation-dipole model and shell model (a) using the same experimental Debye–Waller B values with each model and (b) using Debye–Waller B values calculated by the models themselves.

Multiphonon scattering near Bragg reflections

The preceding figures lead to several observations about multiphonon scattering in the vicinity of Bragg reflections. For all but the lowest-index reflections it exists in plenty at room temperature for a typical material considered here. It has structure, peaking under the reflection but not peaking as strongly as the one-phonon. Hence at the resolution of these calculations the peak is not particularly well shown. The important practical point, however, is that the volume of reciprocal space sampled by many detectors is such that they collect diffuse scatter substantially away from Bragg reflections, well into the region where for higher $\sin\theta/\lambda$ multiphonon processes dominate the diffuse scattering. The corollary to this is that if corrections are to be based on the principle that the one-phonon TDS is the most important (in terms of structure, if not magnitude), the sampled volume of reciprocal space must be kept as small as possible by using a narrow detector slit, a small crossfire beam, well monochromated radiation and a crystal of reasonably small mosaic spread. These precautions are just those one should take in any case to improve the 'signal-to-noise ratio' of Bragg scattering to diffuse scattering.

The other important feature of multiphonon scattering is that as a ratio to Bragg scattering it increases roughly exponentially with temperature in the high-temperature limit, as opposed to the linear increase of one-phonon scattering. Setting $\mathbf{K} = \mathbf{G}$, a reciprocal-lattice vector, in the calculation described here gives for the total phonon scattering the sum of true multiphonon processes ending on $\mathbf{G}$ and the average scattering from all processes involving zerophonon wavevectors in the volume V_Z. Moreover, the Bragg scattering that is calculated is not the integrated Bragg scattering but the peak of the diffraction pattern due to the microcrystal. However, following the arguments of Willis (1969) it is found that the ratio of diffuse scattering to Bragg scattering so calculated is just the ratio of *integrated* diffuse scattering to Bragg scattering seen by a counter of resolution V_Z. The average one-phonon contribution (I_1) is correctly represented, within the approximations of the zerophonon treatment, as

$$I_1/N\sigma_0 I_0 = N \sum_{kk'} f_k \exp(-W_k) f_{k'}^* \exp(-W_{k'}) \times \exp\{i\mathbf{G} \cdot [\mathbf{r}(0k) - \mathbf{r}(0k')]\} Z_{kk'} \quad (17)$$

since the only phonons that contribute to this scattering are within the zerophonon volume. Multiphonon processes seen by such a counter are also included, but less accurately. Table 2 gives a quantitative illustration for some reflections from GaAs at 295 and 700 K of values for the Bragg intensity (I_B), the one-phonon intensity (as a percentage of I_B) and the multiphonon intensity I_m (also as a percentage), the

Table 2. *Intensities given by the calculation when* **K** *is set to a Bragg reflection hkl*

The phonon intensities are related to the integrated intensities recorded by a counter that sees a surrounding spherical volume V_Z in reciprocal space (see text). The calculation has been made with an $n=4$ cubic mesh (giving $V_Z = 1/256$ of the Brillouin zone volume), for GaAs at 295 and 700 K. I_B is the Bragg intensity in electron units (e.u.) per cell; I_1 the one-phonon intensity [essentially from equation (17)] and I_m the multiphonon intensity calculated as the difference between the total phonon scattering and I_1. It can be seen that, as a rule of thumb, the weaker is the reflection the larger is I_1/I_B and the larger is I_m/I_1.

Reflection			295 K			700 K		
h	k	l	I_B (e.u./cell)	$100I_1/I_B$ (%)	$100I_m/I_B$ (%)	I_B (e.u./cell)	$100I_1/I_B$ (%)	$100I_m/I_B$ (%)
5	5	5	$2{\cdot}99\times10^4$	7·2	0·42	$1{\cdot}02\times10^4$	17·1	2·72
6	6	6	$2{\cdot}25\times10^2$	35·1	12·6	1·68	1974	3200
7	7	7	$7{\cdot}15\times10^3$	14·2	1·84	87	362	159
8	8	8	$7{\cdot}69\times10^3$	18·3	2·97	498	50·4	30·4
6	6	0	$6{\cdot}26\times10^4$	6·8	0·35	$2{\cdot}23\times10^4$	16·2	2·18
5	3	1	$8{\cdot}91\times10^4$	3·35	0·09	$5{\cdot}39\times10^4$	7·9	0·51
10	6	4	$1{\cdot}36\times10^4$	14·4	1·72	$1{\cdot}56\times10^3$	36·1	13·8

calculation taking the observed volume as 1/256th of the Brillouin zone. The results can be scaled to other volumes following Reid (1973).

A somewhat different interpretation of what scattering processes are happening close to Bragg peaks is provided by the observation made earlier that the zerophonon term cancels the zerophonon contribution to the Debye-Waller factor. In fact the entire TDS at $\mathbf{K}=\mathbf{G}$ cancels the $\mathbf{q}=0$ contribution to the Debye-Waller factor. In general the TDS from a small volume around the reciprocal-lattice point cancels the Debye-Waller reduction in the Bragg reflection caused by the small wavevector modes in that volume. The net effect is that there is no effect of low-wavevector phonons on Bragg intensities. In other words, for a counting system that necessarily integrates not only the Bragg intensity but diffuse scattering from a surrounding region, Bragg scattering will be observed that is not reduced by the full Debye-Waller factor but only by the contribution to the Debye-Waller factor of all modes lying *outside* the sampled volume of reciprocal space. This interpretation is valid provided the sampled volume contains phonons reasonably well represented by the dispersionless limit. For larger wavevector phonons, the diffuse scattering involving $\mathbf{K}=\mathbf{G}-\mathbf{q}$ is not equal to the loss of Bragg scattering caused by the $\mathbf{q}$ phonons contributing to the Debye-Waller factor.

Looked at in real-space terms, there is never a Debye-Waller reduction of intensity merely from a translation of the whole crystal backwards and forwards. For an apparatus whose resolution extends a short distance $\mathbf{q}_s$ away from reciprocal-lattice points, there is also a negligible reduction of Bragg intensity due to all lattice waves of wavelength longer than $2\pi/\mathbf{q}_s$. Perhaps this interpretation can be made the basis of an alternative intensity correction strategy involving the calculation of partial Debye-Waller factors.

Multiphonon scattering from a deforming electron distribution

The use of a shell model to calculate the scattering from a deforming electron distribution has recently received some quantum mechanical justification by Matthew & Yousif (1984). Reid (1983*b*) examined what effect such deformations are likely to have on the Debye-Waller factor for Bragg reflections, giving numerical results for a number of cubic zincblende structure materials. Do these ionic deformations also alter the total phonon scattering? Application of the same first-principles approach with a shell model leads to a modified phonon scattering cross section, which could be evaluated without approximation in the spirit of this paper. However the precise evaluation would be time consuming and it is clear that the additional terms are controlled by the shell scattering factor, which typically dies away at $\sin\theta/\lambda$ around 0·15 Å^{-1}. Hence in the region where the total phonon scattering may be significantly affected by a deforming electron distribution, multiphonon processes are of little importance and the scattering is dominated by the one-phonon cross section. It is appreciably simpler to incorporate ionic deformation in the one-phonon cross section only, and examples of its effects can be seen in the calculations of Reid (1974).

I would like to thank the Science and Engineering Research Council for grant support during this work and Aberdeen University Computing Centre for providing the computing facilities.

APPENDIX

Notation for the scattering cross section

I/I_0	ratio of scattered to incident intensity
N	number of unit cells in scattering sample

σ_0	scattering given by a free electron
l	index labelling unit cells
k	index labelling atom within unit cell
f_k	scattering factor
W_k	Debye-Waller term $= (1/2N)\sum_\lambda (E/\omega^2)_\lambda \lvert\mathbf{K}\,.\,\mathscr{E}(k/\lambda)/m_k^{1/2}\rvert^2$
$\mathbf{K}$	scattering vector
$\mathbf{r}(lk)$	equilibrium coordinate of atom (lk)
λ	phonon state label $(\mathbf{q}j)$
$\mathbf{q}$	phonon wavevector
j	phonon branch index
ω_λ	phonon angular frequency
E_λ	average energy in phonon state $(\mathbf{q}j)$
m_k	mass of kth atom in unit cell
$\mathscr{E}(k/\lambda)$	(normalized) eigenvector for atom type k and phonon state λ

References

BORN, M. (1942). *Rep. Prog. Phys.* **9**, 294-333.
GHEZZI, C. & BOCCHI, C. (1982). *Thin Solid Films*, **88**, 1-8.
International Tables for X-ray Crystallography (1974). Vol. IV. Birmingham: Kynoch Press. (Present distributor D. Reidel, Dordrecht.)
MARADUDIN, A. A., MONTROLL, E. W. & WEISS, G. H. (1963). *Theory of Lattice Dynamics in the Harmonic Approximation*, pp. 231-251. *Solid State Physics Suppl.* No. 3. London: Academic Press.
MATTHEW, J. A. D. & YOUSIF, S. Y. (1984). *Acta Cryst.* A**40**, 716-721.
ORLOVA, N. S. (1979*a*). *Phys. Status Solidi B*, **93**, 503-509.
ORLOVA, N. S. (1979*b*). *Sov. Phys. Crystallogr.* **24**, 516-518.
ORLOVA, N. S. (1981). *Phys. Status Solidi B*, **103**, 115-121.
REID, J. S. (1973). *Acta Cryst.* A**29**, 248-251.
REID, J. S. (1974). *Phys. Status Solidi B*, **64**, 57-64.
REID, J. S. (1983*a*). *Acta Cryst.* A**39**, 1-13.
REID, J. S. (1983*b*). *Acta Cryst.* A**39**, 533-538.
REID, J. S. & SMITH, T. (1970). *J. Phys. C*, **3**, 1513-1526.
ROBERTSON, B. F. & REID, J. S. (1978). *Acta Cryst.* A**35**, 785-788.
WALLER, I. (1928). *Z. Phys.* **51**, 213-231.
WILLIS, B. T. M. (1969). *Acta Cryst.* A**35**, 277-300.

Acta Cryst. (1985). A**41**, 528-530

A Note on the Superspace Groups for One-dimensionally Modulated Structures

BY AKIJI YAMAMOTO*

National Institute for Research in Inorganic Materials, Sakura-mura, Niihari-gun, Ibaraki, 305, *Japan*

T. JANSSEN AND A. JANNER

Institute for Theoretical Physics, University of Nijmegen, 6525 *ED Nijmegen, The Netherlands*

AND P. M. DE WOLFF

Vakgroep Fysische Kristallografie, Laboratory for Technical Physics, Technische Hogeschool, 2628 *CJ Delft, The Netherlands*

(*Received* 5 *December* 1984; *accepted* 10 *May* 1985)

Abstract

A computer generation of all the non-equivalent superspace groups for one-dimensionally modulated structures has been performed. Comparison of this result with the previous list by de Wolff, Janssen & Janner [*Acta Cryst.* (1981), A**37**, 625-636] shows that three superspace groups in this list are equivalent to others and that six groups had been overlooked. The new list contains 775 (3+1)-dimensional superspace groups. Some ambiguous points in the notation of the superspace groups and the selection of the wave vector are discussed.

1. Corrections to the former list

A list of (3+1)-dimensional superspace groups has been given by de Wolff, Janssen & Janner (1981), hereafter referred to as I. The list was calculated partly by computer, partly by hand. Although the calculation was done carefully and employing two independent methods, errors are almost unavoidable in computations of such length by hand. For that reason we have once more executed the calculations of the non-equivalent superspace groups in which all the steps were performed by means of a computer. Furthermore, in order to remove errors in programming, superspace groups have been generated by two independent programs based on the same theory (Janner & Janssen, 1979). As a result, several discrepancies have been found between the new list and

* This work was partly done, while on leave, as a visiting member of the Institute for Theoretical Physics, University of Nijmegen.

0108-7673/85/060528-03$01.50